Neuron, Volume *104*

Supplemental Information

Xenotransplanted Human Cortical Neurons Reveal Species-Specific Development and Functional Integration into Mouse Visual Circuits

Daniele Linaro, Ben Vermaercke, Ryohei Iwata, Arjun Ramaswamy, Baptiste Libé-Philippot, Leila Boubakar, Brittany A. Davis, Keimpe Wierda, Kristofer Davie, Suresh Poovathingal, Pier-Andrée Penttila, Angéline Bilheu, Lore De Bruyne, David Gall, Karl-Klaus Conzelmann, Vincent Bonin, and Pierre Vanderhaeghen

Supplemental Information

Xenotransplanted human cortical neurons reveal species-specific development and functional integration into mouse visual circuits

Daniele Linaro, Ben Vermaercke, Ryohei Iwata, ..., Vincent Bonin, and Pierre Vanderhaeghen

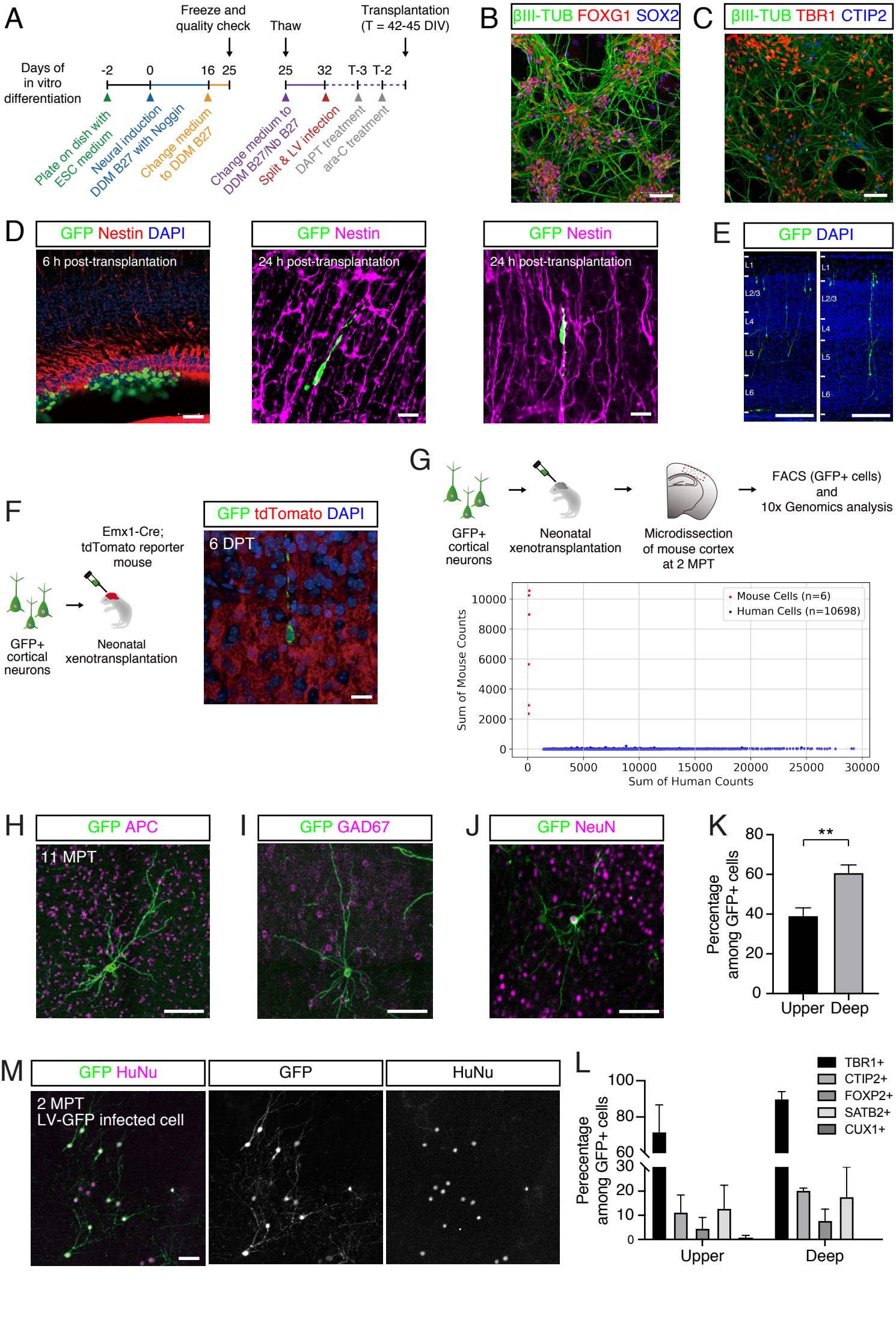
A
Freeze and quality check
Thaw
Transplantation (T = 42-45 DIV)
Days of in vitro differentiation
-2
0
16
25
25
32
T-3
T-2
Plate on dish with ESC medium
Neural induction DDM B27 with Noggin
Change medium to DDM B27
Change medium to DDM B27/Nb B27
Split & LV infection
DAPT treatment
ara-C treatment
B
βIII-TUB FOXG1 SOX2
C
βIII-TUB TBR1 CTIP2
D
GFP Nestin DAPI
6 h post-transplantation
GFP Nestin
24 h post-transplantation
GFP Nestin
24 h post-transplantation
E
GFP DAPI
L1
L2/3
L4
L5
L6
F
Emx1-Cre; tdTomato reporter mouse
GFP+ cortical neurons
Neonatal xenotransplantation
GFP tdTomato DAPI
6 DPT
G
GFP+ cortical neurons
Neonatal xenotransplantation
Microdissection of mouse cortex at 2 MPT
FACS (GFP+ cells) and 10x Genomics analysis
Mouse Cells (n=6)
Human Cells (n=10698)
Sum of Mouse Counts
Sum of Human Counts
H
GFP APC
11 MPT
I
GFP GAD67
J
GFP NeuN
K
Percentage among GFP+ cells
Upper
Deep
M
GFP HuNu
GFP
HuNu
2 MPT
LV-GFP infected cell
L
Perecentage among GFP+ cells
TBR1+
CTIP2+
FOXP2+
SATB2+
CUX1+
Upper
Deep

Figure S1. Characterization of hESC-derived transplanted cortical neurons, related to Figure 1.
(A) Detailed timeline of the differentiation protocol used to obtain human cortical pyramidal neurons for transplantation in the mouse cortex. (B,C) In vitro validation of the quality of the differentiated cells: at DIV32, most neuronal cells express markers of cortical identity, including FoxG1, Tbr1, CTIP2. Scale bar, 50 µm. (D) Examples of transplanted cells at early time-points (6 and 24 hours) following transplantation illustrating GFP+ transplanted cells invading the ventricular zone and migrating along the Nestin+ radial glia scaffold. (E) Examples of ESC-derived cortical neurons at 9 days post-transplantation integrated in the mouse cortex throughout the 6 cortical layers. Scale bar, 200 µm. (F) Left: Transplantation paradigm to test host-transplant cell fusion. Right: Example of isolated GFP+/tdTomato- ESC-derived cortical neurons in GFP-/tdTomato+ mouse brain at 6 DPT. (tdTomato+ cells among GFP+ cells, 0/40 cells from 3 mice). (G) TOP: Scheme representing FACS and scRNA-seq analysis to test host-transplant cell fusion. Bottom: FACS-sorted cell identified as human or murine based on scRNA-seq reads that mapped to the human (x-axis) and mouse (y-axis) genome alignment. Isolated human cells display no mouse sequence reads, while mouse control cells display no human sequence reads (10704 cells from 2 mice). (H) Example of transplanted human cells at 11 MPT negative for astrocyte and oligodendrocyte marker APC (APC positive cells among GFP+ cells: 0/19 cells from 2 mice). (I) Example of transplanted human cells negative for GAD67 (GAD67 positive cells among GFP+ cells: 0/27 cells from 2 mice). (J) Examples of transplanted human cells at 11 MPT positive for neuronal marker NeuN (NeuN positive cells among GFP+ cells, 29/29 cells from 2 mice). (K) Distribution of GFP+ transplanted cells in upper (2/3/4) and deep (5/6) layers (1214 cells from 2 mice). (L) Proportion of human cells positive for several cortical markers in upper (2/3/4) or deep (5/6) layers (TBR1 positive cells: among 79 GFP+ cells in upper layers and 59 GFP+ cells in deep layers; CTIP2 positive cells: among 168 GFP+ cells in upper layers and 370 GFP+ cells in deep layers; FOXP2 positive cells: among 69 GFP+ cells in upper layers and 180 GFP+ cells in deep layers; SATB2 positive cells: among 51 GFP+ cells in upper layers and 138 GFP+ cells in deep layers; CUX1 positive cells: among 48 GFP+ cells in upper layers and 52 GFP+ cells in deep layers)t. (M) ESC-derived cortical neurons were infected in vitro with lentivirus transducing eGFP, and transplanted two weeks later. Example of transplanted cells integrated in the mouse cortex at 2 MPT labeled for human specific nuclear antigen (human nuclei positive cells among GFP+ cells, 61/61 cells from 2 mice). Scale bars: (B,C) 50 µm. (D) 50 µm (left), 20µm (middle, right). (E) 200 µm. (F) 20 µm. (H-J) 100 µm. (M) 50 µm. Markers and error bars indicate mean ± SEM. *$p<0.05$; **$p<0.01$; Mann-Whitney U test.

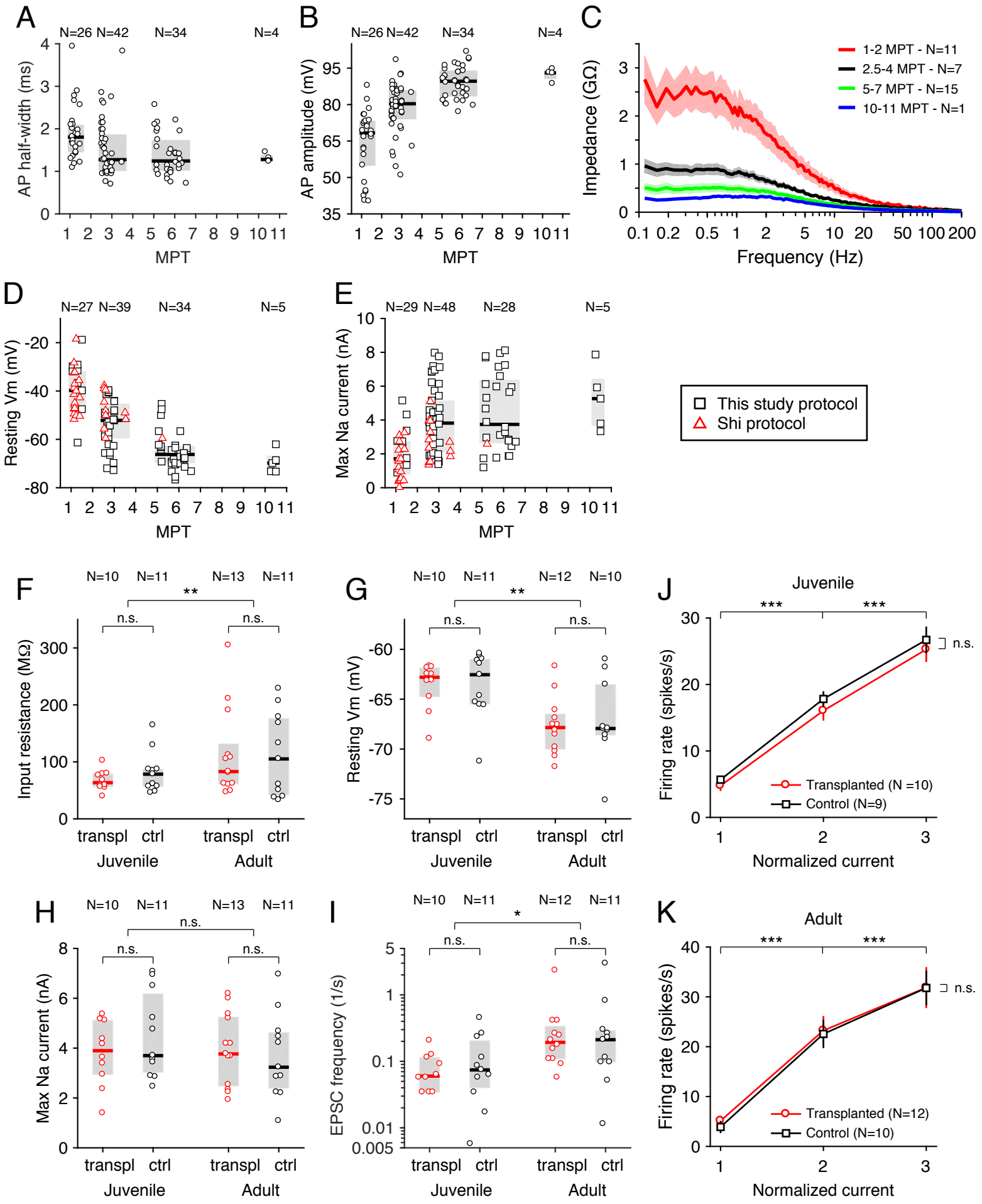
A
N=26 N=42 N=34 N=4
AP half-width (ms)
MPT
B
N=26 N=42 N=34 N=4
AP amplitude (mV)
MPT
C
1-2 MPT - N=11
2.5-4 MPT - N=7
5-7 MPT - N=15
10-11 MPT - N=1
Impedance (GΩ)
Frequency (Hz)
D
N=27 N=39 N=34 N=5
Resting Vm (mV)
MPT
E
N=29 N=48 N=28 N=5
Max Na current (nA)
MPT
This study protocol
Shi protocol
F
N=10 N=11 N=13 N=11
Input resistance (MΩ)
n.s.
**
transpl ctrl transpl ctrl
Juvenile Adult
G
N=10 N=11 N=12 N=10
Resting Vm (mV)
n.s.
**
transpl ctrl transpl ctrl
Juvenile Adult
J
Juvenile
***
n.s.
Firing rate (spikes/s)
Transplanted (N =10)
Control (N=9)
Normalized current
H
N=10 N=11 N=13 N=11
Max Na current (nA)
n.s.
transpl ctrl transpl ctrl
Juvenile Adult
I
N=10 N=11 N=12 N=11
EPSC frequency (1/s)
*
n.s.
transpl ctrl transpl ctrl
Juvenile Adult
K
Adult
***
n.s.
Firing rate (spikes/s)
Transplanted (N=12)
Control (N=10)
Normalized current

Figure S2. Electrophysiological properties of hESC-derived transplanted cortical neurons and mouse L5 cortical pyramidal cells, related to Figure 2.
(A,B) Development of action potential half-width and amplitude over the course of 11 MPT. Values attained at the end of this developmental period are comparable to those observed in human ex vivo samples. (C) Membrane impedance as a function of stimulating frequency at 4 consecutive developmental stages. Notice how the overall impedance decreases with time, in line with the reduction of input resistance observed in the same cells. (D,E) Development of resting membrane potential and maximum recorded sodium currents as a function of time, for two distinct differentiation protocols. Notice how the choice of differentiation protocol does not seem to affect the overall pace of development of the cells. (F-I) Input resistance, resting membrane potential, maximal sodium current and frequency of spontaneously incoming EPSCs in cortical L5 pyramidal cells of NOD/SCID mice at two time points (juvenile, post-natal day (P)14-15, and adult P40-42) in transplanted (red circles) and control animals (black circles). No significant differences were found between transplanted and control animals at either age, while most of the properties shown here and others we tested were significantly correlated with the age of the animal. Each marker represents the value of a property for a single cell, horizontal lines are median values and grey shaded areas represent interquartile ranges. The number of cells is shown above each column. *$p < 0.05$; **$p < 0.01$, two-way ANOVA. (J-K) Static input-output f-I curves of L5 pyramidal cells in transplanted (red circles and lines) and non-transplanted (black squares and lines) NOD/SCID at two different ages (P14-15 and P40-42). Input current is normalized to the measured value of minimal current sufficient to elicit firing in each cell. No significant differences were observed between transplanted and control animals at either age. Markers and error bars indicate mean ± SEM. ***$p < 0.001$, ANOVA for mixed design, with the current level as within-subject and the experimental condition (transplanted vs. control) as between-subject factor.

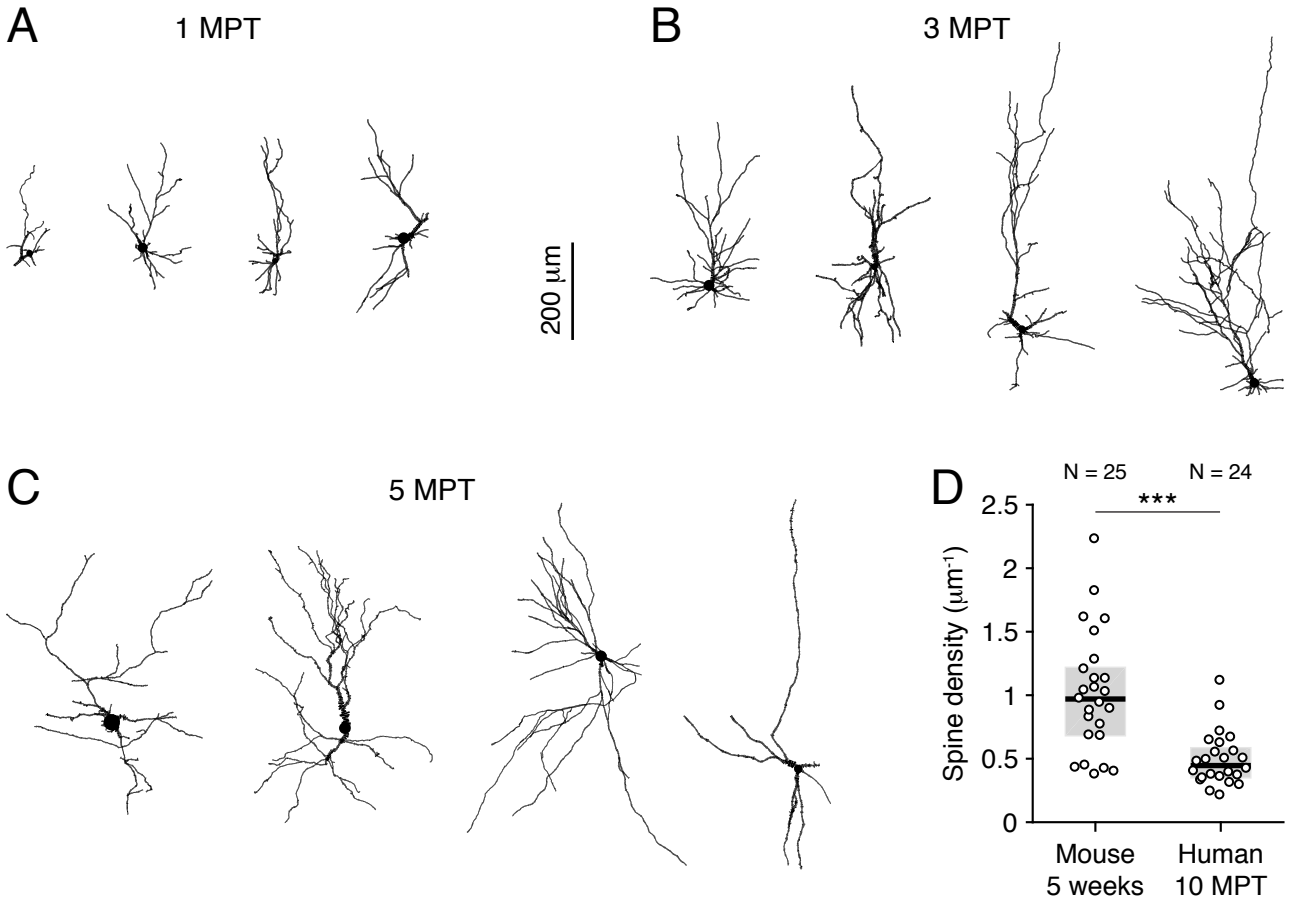

Figure S3. Representative human cell morphologies at various developmental stages and dendritic spine density, related to Figure 3.

(A-C) Four digitally reconstructed cell morphologies at 1, 3 and 5 MPT. Notice the increase in dendritic complexity and overall length. (D) Comparison of dendritic spine density between mouse cortical neurons at 5 weeks of age and human transplanted neurons at 10 MPT. ***p<0.001, Mann-Whitney U test.

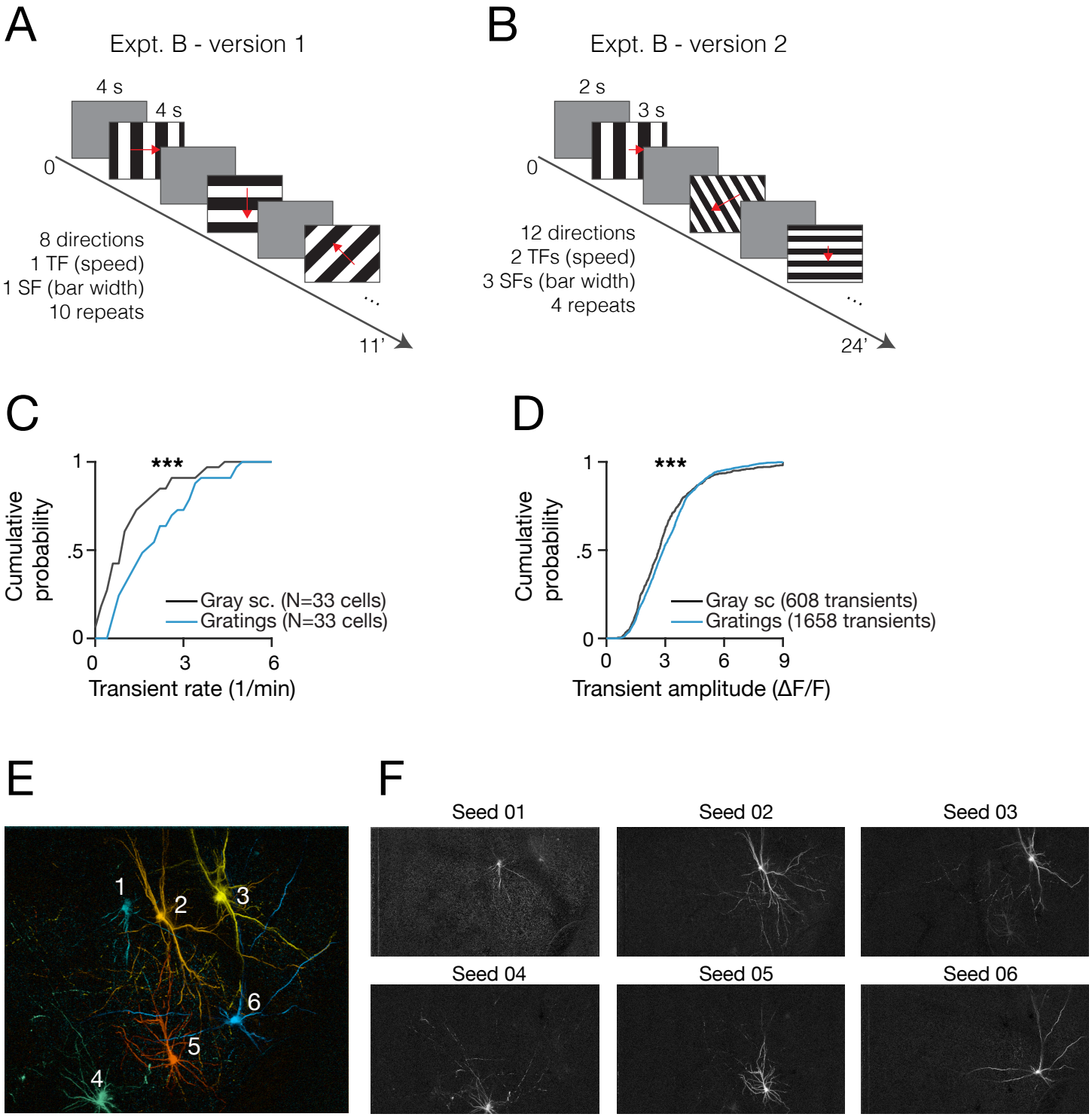

Figure S4. In vivo calcium imaging experimental paradigm, related to Figure 6.
(A,B) Description of the visual paradigms used in this study. (A) In version 1, gratings (SF=0.05 cpd, TF=4 Hz) drifted in 8 directions. (B) In version 2, we used gratings drifting in 12 direction in combinations of two TFs (1 and 4 Hz) and three SFs (0.04, 0.08 and 0.16). (C,D) Cumulative distributions for transient rate and amplitude for matched cells recorded during grey screen and visual stimulation. (E) Maximum intensity projection of seeded correlation maps for 6 neurons. (F) Individual seeded correlation maps. To generate these maps, we correlated the average fluorescence trace of each "seed" neuron with the time course of every pixel in the movie. These correlation values are then collapsed into a single 2D image that provides a detailed image of the morphology of the seed neuron.

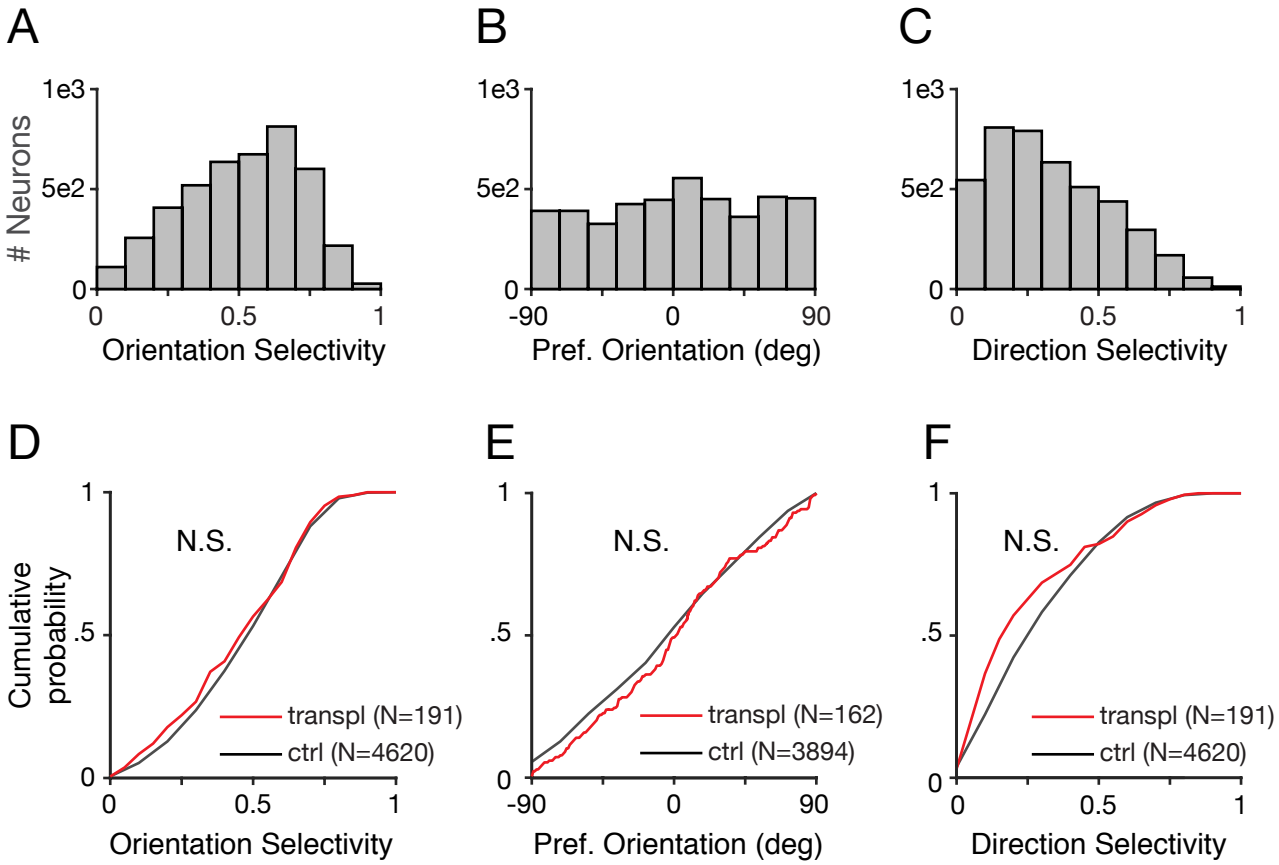

Figure S5. Response properties of mouse neurons during visual stimulation, related to Figure 7.
(A-C) Probability distributions of 4620 mouse (mouse line: CaMKll-tTA x TRE-GCamp6.lineG6s2) L2/3 V1 pyramidal neurons for (A) preferred orientation, (B) orientation selectivity index and (C) direction selectivity index. These same data are presented as reference in Figure 7B-D. (D-F) Comparison of same 3 response indices for cells recorded in control (black lines) and transplanted (red lines) animals, showing that our procedures do not affect responses of host cells. Control data is also presented in A-C and Figure 7B-D.